Studying the Kinematics of the Neutral Gas in the Extraplanar of the Milky Way

Ameerah Ab. Al-Sadooni[1*], Ghaidaa A. Hafedh Jaber[2], Wasnaa Witwit[3]

Abstract

The study is based on the Parkes Galactic All Sky Survey (GASS III) to investigate the neutral hydrogen (H I) emission in the areas surrounding the disc of the Milky Way (MW). The aim of the study is to looking for a sign of disk-halo interaction by tracing the kinematics of the H I in different heights from the midplane of the MW, as a spiral galaxy. The analysis focused on the 21 cm spectral line to examine the shape of the emission line and determine the Gaussian parameters according to the number of fitting functions. Twelve positions were investigated by chosen two slices with longitude (l = 20̊, 340̊) and different latitude (b = 10̊, 12̊, 14̊, 16̊, 18̊, 20̊) for each slice. In some positions the line profiles show broadening or even line splitting as a result to interaction between different component with different kinematics and physical environments. Our results also indicate that the velocity reduces with increase the height from the midplane and take this as evidence of lags as a result to the interaction between the disk and halo.

Key Words: Galaxy, Disc-halo Interaction, Lags, Kinematics, HI, Disc.

DOI Number: 10.14704/nq.2022.20.3.NQ22050 **NeuroQuantology 2022; 20(3):111-117**

Introduction

Spiral galaxies show a thin disc that consists of neutral hydrogen (H I), and it can extend radially away from the optical radius. The typical scale-height of the H I disc in the inner regions is between 100 pc to 200 pc. This range is well described by adopting a vertical hydrostatic equilibrium between the gas and galactic potential. In other words, the gravitational force of the stellar disc and halo balance the turbulent motions of the gas (Olling *et al,* 2002). The H I layer in the outer regions of the disc is assumed to flare as a result to the rise of the vertical force, while the scale-height of the optical radius unexpected to be more than a factor two (Bacchini *et al*, 2019). Then we expected the inner part of the disc, which shows the high starfomation rate, to be limited for a few hundred parsec.

The later expectation not agree with the H I observation in such galaxies, where a thick layer of H I (≤ 10% of H I component) extended more than a few kiloparsecs above the midplain (Fraternali *et al*, 2002; Oosterloo *et al*, 2007). This layer is named extraplanar gas, and shows slowly rotating gas comparing with the gas in the disc (Schaap *et al*, 2002; Zschaechner *et al*, 2011). In spiral (disc) galaxies, the ionized hydrogen component is traced in extraplanar also, and extended a few kpc from the disc with ~ 10^4 K (Rossa *et al*, 2003). The ionized extraplanar is highly prominent in galaxies with high starformation rate (Veilleux *et al*, 2003). The formation of the extraplanar has been studied in different mechanisms that fall into three models including: equilibrium (Barnabè *et al*, 2006), which failed to reproduce the observed data of NGC 891in cool environment by the suggested model.

Corresponding author: Ameerah Ab. Al-Sadooni
Address: [1*2,3]Department of Physics, College of Science, University of Babylon, Babel, Iraq.
[1*]E-mail: ameerahalsadooni@yahoo.com
Relevant conflicts of interest/financial disclosures: The authors declare that the research was conducted in the absence of any commercial or financial relationships that could be construed as a potential conflict of interest.
Received: 30 December 2021 **Accepted:** 02 February 2022

The gas accretion from the external environment was the second mechanism that was adopted to reproduce kinematics of accreting gas almost is similar to that one in NGC 891(Kaufmann *et al*, 2006). However, this model failed to balance the accretion rate of the gas and the star-formation rate (Fraternali *et al*, 1976). The galactic fountain model another mechanism that would produce the extraplanar. When superbubble expand by swept up gas from the disc as a result to the impact of the supernova and stellar winds around OB associations (Shapiro *et al*, 1976; Collins *et al*, 2002). In case that the scale-height of the superbubble exceed that one of the typical disc it would blow out and then the hot gas in the superbubble and the cold gas that gathered in the shell of the superbubble will eject into the halo. The most material of the extraplanar of H I is made up from the supershells, while the hot ejected gas after cooling which contributes partially (Houck *et al*, 1990). The extent of the H I extraplanar in the MW and NGC 891 can be reproduced successfully in these models and show a sign of disc- halo interaction (Fraternali *et al*, 2013; Fraternali *et al*, 2017).

The Parkes Galactic all-sky survey presents data that traced 21 cm spectral line of atomic (H I) for the sky surrounding the MW. This survey helps to probe all areas that surrounding the MW and are inaccessible to observe at any other wavelengths, as 21 cm line has valuable advantages (will talk about later). Then GASS III data will be an excellent environment to investigate the kinematics of the extraplaner and look for any sign of disk-halo interaction in the MW. The paper is organized as follows: the the Parkes Galactic All Sky Survey (GASS) and the data reduction are presented in Sect. II. The results are analyzed and discussed in Sect. III. Sect. IV shows the conclusion.

Observations, Data Processing and Results

A. The Parkes Galactic All Sky Survey (GASS)

The data of the survey were collected with the Parkes Radio telescope with 64-m which is one of the largest single-dish telescopes in the southern hemisphere and one instruments of the Australia Telescope National Facility. The first stage of GASS survey represented survey goals and techniques of observations (McClure-Griffiths *et al*, 2009). While the second one focused on the stray radiation and instrumental corrections (Kalberla *et al*, 2010) and finally the third data release (GASS III) is clean from any instrumental effects (Kalberla *et al*, 2015). This survey covers the southern sky of the MW ($\delta \geq 1°$) to trace the atomic hydrogen, 2π steradians were covered by the survey and the gridded angular resolution is about 16'. The observed data traced velocity range between -400 km s^{-1} to -400 km s^{-1} with 1 km s^{-1} as a velocity resolution. The released data from the GASS III survey is as 3D FITS data cubes.

B. Data Reduction

The 3D FITS data cube was downloaded from the web interface of the GASS III survey www.astro.uni-bonn.de/hisurvey/AllSky_gauss/. The downloaded cube covers a part of the sky that is between the longitude -20° to 20° and the latitude from 0° to 20°, as shown in Figure 1. We used the data cube to study the intensity of 21 cm profile as a function of the radial velocity in two different latitude (20° and 340°). The first step was to test a slice in the MW with longitude (l) equals to 20° and chosen a range of latitude (10° to 20°) in equally spaced 2° bins. The second step was to choose another slice with l = -20° and test different latitude from 10° to 20° in equally step (2°).

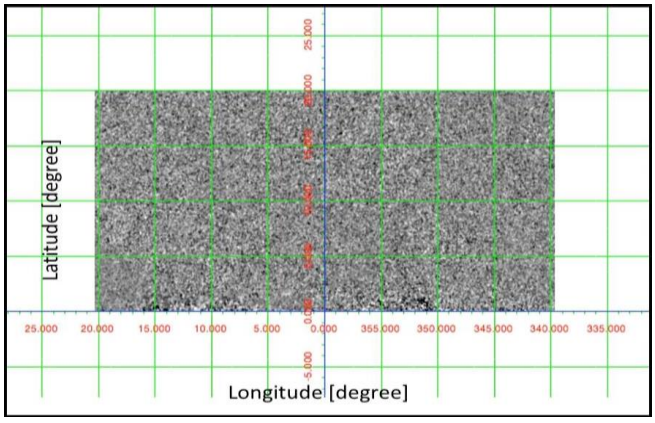

Fig. 1. The projection of the 3D FITS data cube which represent the selected area in this study

Analysis and Discussion

A. The Radio Emission Line 21 cm

The 21 cm is a hyperfine transition line of the neutral hydrogen between the two 1s states. The rest frequency of the line is 1420.4057 MHz and wavelength ≈ 21.1061 cm.

The excellent advantages of 21 cm line that it can observed directly and as a long wavelength it is not scattered through passing dusty region. Furthermore the 21 cm introduced a controversial view not only related to physical and kinematical proportions of ISM, but also about the distribution

of dark matter, rotational curve, and warped plane in the Milky Way. In other words it helps to introduce global map for the structure of the galaxy (Levine *et al*, 2006) as well as widely various galactic processes could be traced efficiently by λ=21 cm spectral line.

B. Emission Line Profile Measurements

The spectra of each position was extracted from the 3D cube by using ds9, and analysed using Python to fit and plot. The profile of the neutral atomic hydrogen (H I) 21 cm of each region was plotted and examined to show the shape of the profiles and separate Gaussian components. The emission lines were fit with Gaussian component. The selected positions show different shapes of 21cm line profiles, some exhibit splitting or significant broadening of their profiles. Therefore, a combination of two or more Gaussian functions were fit to the line profiles of these positions as shown in Figures 2 and 3.

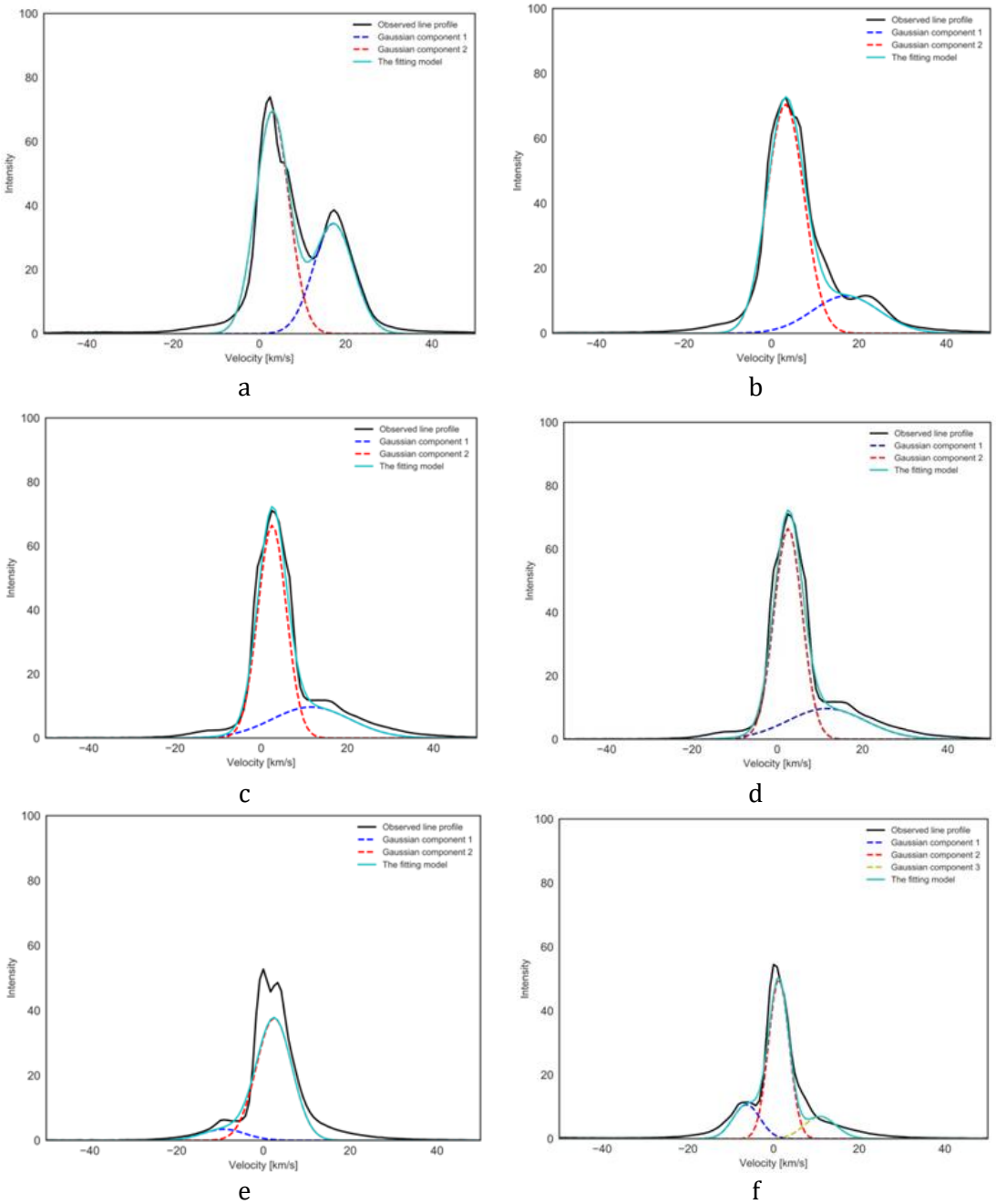

Fig. 2. The 21cm emission line and fitted profile: panels from a to f show the 21 cm profile and model fit at (l = 10̊,12̊, 14̊, 16̊,18̊, 20̊) respectively, with B = 20̊

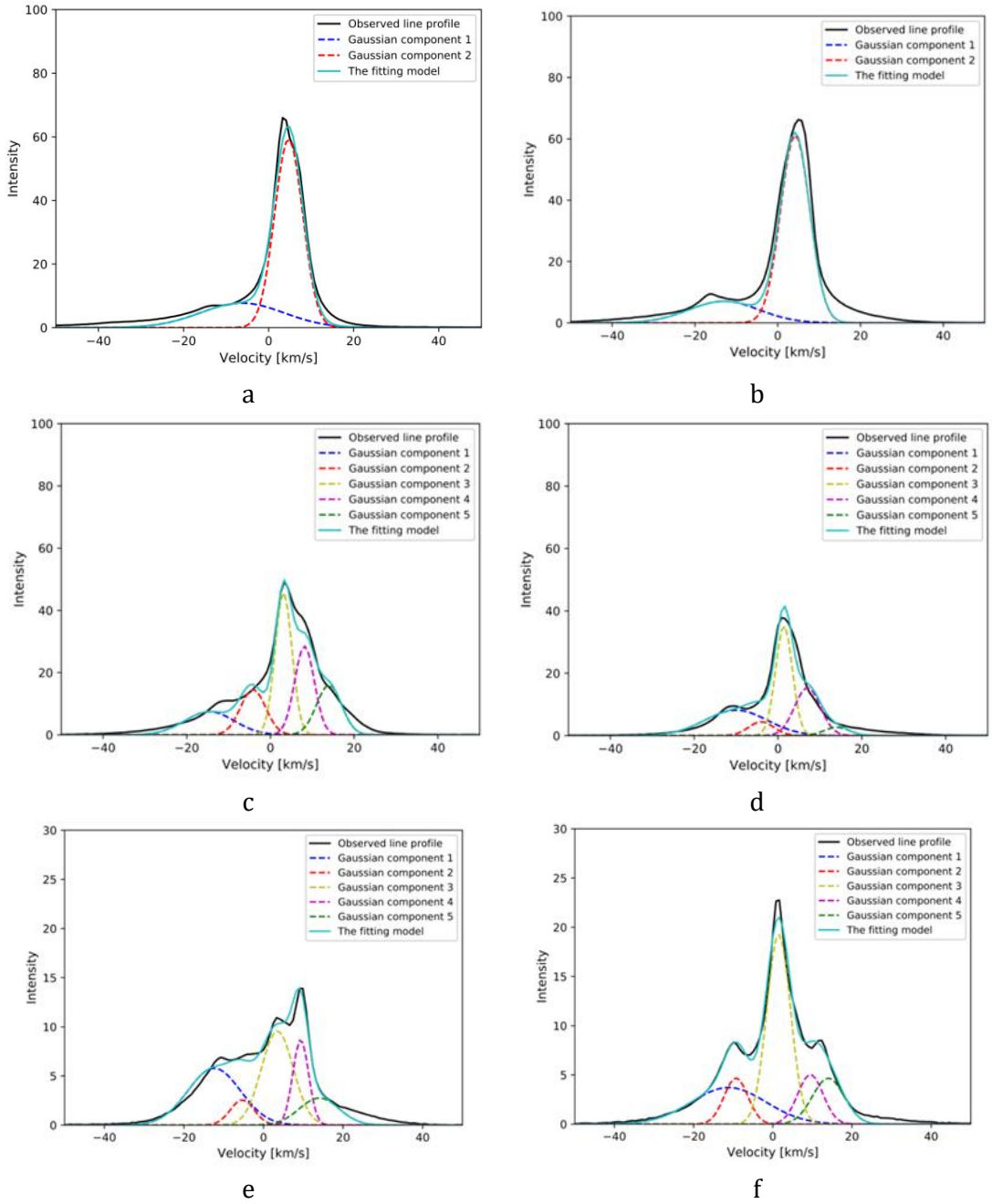

Fig. 3. The 21cm emission line and fitted profile: panels from a to f show the 21 cm profile and model fit at (l = 10̊,12̊, 14̊, 16̊,18̊, 20̊) respectively, with B = 340̊.

C. Kinematics of the Neutral Gas (H I)

Gas kinematics were examined within each selected position via the Doppler effect along the line-of-sight. The radial velocities and velocity dispersion were determined for each component of the emission line by using Gaussian parameters of the fits, and are listed in Table I and II. In general, we notice that it is impossible to fit the profile of the emission line by one Gaussian function, and the profile in each position proposes different shape.

Table I. Centroid velocity and full-width at half maximum of 21cm emission-line in different latitude with longitude = 20 degree

Longitude = 20 degree				
	First component		**Second component**	
Latitude	**Velocity**	**FWHM**	**Velocity**	**FWHM**
degree	**(km s^{-1})**	**(km s^{-1})**	**(km s^{-1})**	**(km s^{-1})**
10	17±1	11±1.5	3±0.33	9±0.5
12	17±2	18±0.8	3.2±0.4	10±0.3
14	11.6±2	21±0.5	2.5±0.03	7.8±0.01
16	10±1	14±1	1±0.02	7.7±0.03
18	-9±1	11.5±3	2±0.05	9.7±0.68
20	-6.3±8	7±0.33	2.5±0.04	5.6±0.01

Table II. Centroid velocity and full-width at half maximum of 21 emission-line in different latitude with longitude = 340 degree.

Longitude = - 20 degree										
Latitude	**First component**		**Second component**		**Third component**		**Fourth component**		**Fifth component**	
degree	**km s^{-1})**	**km s^{-1})**	**km s^{-1})**	**km s^{-1})**	**km s^{-1})**	**km s^{-1})**	**km s^{-1})**	**km s^{-1})**	**km s^{-1})**	**km s^{-1})**
0	6 ±0.3	3±0.2	.2±0.02	.7±0.1	…	…	…	…	…	…
2	13=0.2	0±0.4	.2±0.1	.2±0.1	…	…	…	…	…	…
4	14±0.2	3±0.2	4.2±0.3	.1±0.7	.1±0.3	.7±0.3	.1±0.4	.5±0.3	4±0.4	.1±0.3
6	10±0.4	7±0.3	4.1±0.3	.1±0.5	.4±0.3	.8±0.1	.0±0.4	.3±0.3	4±0.5	.1±0.3
8	12±0.3	5±0.6	5.3±0.4	.1±0.5	.5±0.2	.4±0.7	.3±0.3	.7±0.5	4±0.4	1.7±0.2
0	11±0.1	2±0.5	9.3±0.4	.1±0.2	.4±0.1	.6±0.2	.5±0.2	.5±0.2	4±0.5	.4±0.2

1. The First Slice (I = 20)

We can notice a clear split in the profile along the line of sight at b = 10, then two Gaussian functions were used to fit the line and separate the two components which show velocities almost 17 ± 1 km s^{-1} and 3 ± 0.33 km s^{-1} respectively. The appearance of such profile would be explained as interaction between two environments with different properties. The velocity dispersion of each component is ~ 10 km s^{-1}. The next two positions at b = (12, 14) show a red asymmetry in the profile so I fit the line at b = 12 by using two components. The broader and stronger has higher velocity 17 ± 2 km s^{-1} and dispersion velocity ~ 18 ± 0.8 km s^{-1}. While the fainter component displays lower velocity about 3.2 ± 0.4 km s^{-1} dispersion velocity about 10 ± 0.8 km s^{-1}. The higher dispersion velocity along the selected slice appears in the strong component at b = 14. The next position (b = 16) the two component have less velocities and dispersion velocities. The next position at b = 18, the shape of the emission profile has different feature (a blue asymmetry), the faint component displays negative velocity ~ 9 ± 1 km s^{-1}. The last position that examined which shows asymmetry in the two wings red and blue, then it was fitted with three Gaussian functions, as it is clear in panel f Figures 2. In this area the gas shows various kinematics, this outfall and infill gas. The tree components show velocities~ (- 6 ± 0.2, 1.2 ±0.1, 11 ± 1) km s^{-1} and dispersion velocities ~ (7 ± 0.4, 6 ± 1, 9 ± 1) km s^{-1} respectively.

2. The Second Slice (I = 340)

The first position at b = 10 (panels a) the 21 cm profile show a blue asymmetry. The first component is the wider one in the selected positions in this study with dispersion velocity about 23 km s^{-1} and velocity ~ - 6 km s^{-1}. Where b = 12, the Gaussian components show same feature as in later point. The last four points at b = 14, 16, 18, 20 display complicated 21 cm profiles, it looks difficult to fit with one Gaussian function even two or three, then we decided to fit with five Gaussian functions. The first component in the four positions displays a negative velocity (mean ~ -12 km s^{-1}) with dispersion velocity between 13 km s^{-1} to 22 km s^{-1}. The second component has same dispersion velocities (~ 7 ± 1 km s^{-1}) and a negative velocities between – 4 km s^{-1} to - 9 km s^{-1}. The third, fourth and fifth components display a range of positive velocities (1.4 -14) kms^{-1} and dispersion velocity (4-10) km s^{-1}.

3. A Sign of the Disc-halo Interaction

The Figure 4 shows the trained of the components along the tested areas. We can notice a clear vertical gradient in the velocities of the gas (first component-black points in Figure 4), it would be related to lags that reduce the rotation speed with height above or below the midplane (Oosterloo *et al*, 2007; Heald *et al*, 2007), where the flows and interaction between the disc and halo. This lags appears in some spiral galaxies such as NGC 4013. The later shows steep lag by using H I observation and theoretical models (Zschaechner *et al*, 2015). The second component shows steady trends generally.

The second slice (I = 340) exhibits complicated emission profiles (see Figure 3). The first three components display negative gradient. While the last two components do not have clear trends of velocities. Figures 5 and 6 present velocities dispersion, we can notice the first component has the highest value along the first slices comparing with the other components. The average values of velocities dispersion are labeled in the green dashed line in Figures 5 and 6. Interestingly, the highest value of the velocities dispersion along the two slices appears at the same height from the midplaine at b = 14, and has the same value. This

maybe suggests that the gas experiences the same physical processes.

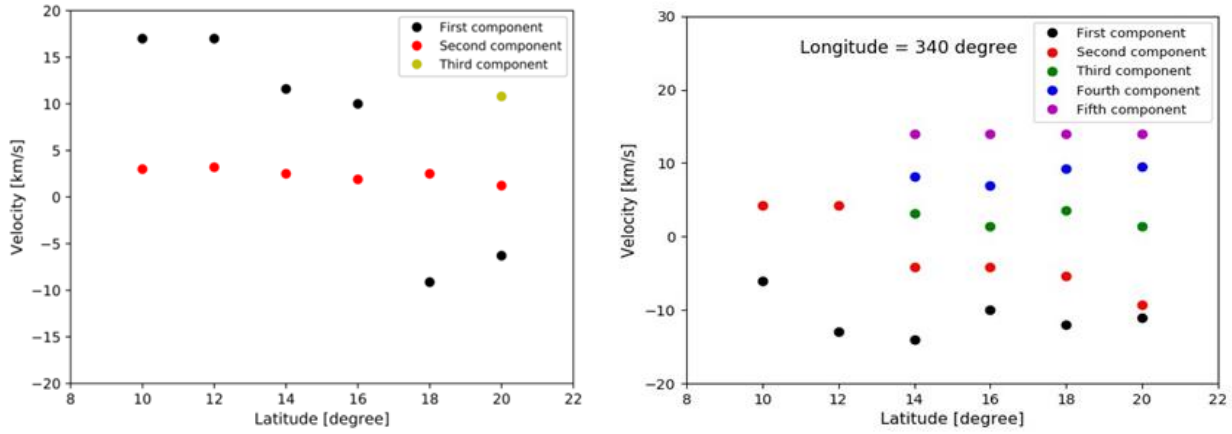

a b

Fig. 4. The two panels represent velocity at (l = 10̊,12̊, 14̊, 16̊,18̊, 20̊), the panel a is at B = 20̊ and panel b at B = 340̊

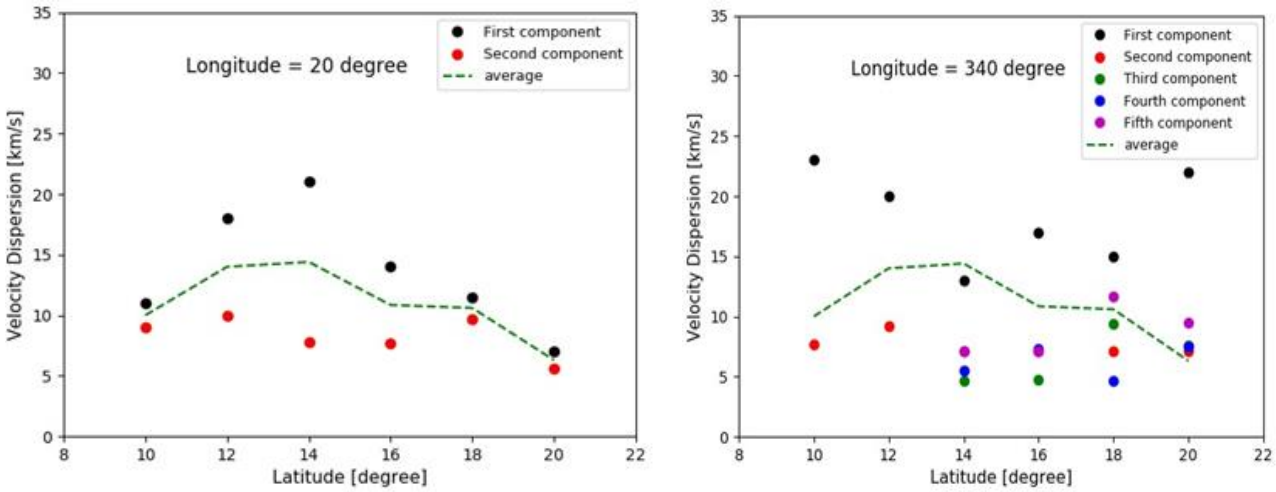

a b

Fig. 5. The two panels represent velocity dispersion at (l = 10̊,12̊, 14̊, 16̊,18̊, 20̊), the panel a is at B = 20̊ and panel b at B = 340̊. The average value are represented by the green dashed line.

Conclusions

The kinematics of the neutral atomic gas were studied at different positions that are away from the midplain of the MW. The profile of the 21 cm emission line in each position was investigated and fitted with Gaussian function (2-5) according to the shape of the profile. The profile shape shows various features such as a red, blue asymmetry or split, and could be understood in terms of interaction with another bulk motion. We study the trends of the velocity (Gaussian components) with increasing latitude and the negative gradient with increasing height from the midplain can be interpreted in terms of lags, as it appears in some disc galaxies.

Acknowledgements

We thank the staff that introduced the Parkes Galactic All Sky Survey (GASS), and we are very appreciate to the University of Babylon for their support during the research.

References

Bacchini C, Fraternali F, Iorio G, Pezzulli G. The volumetric star formation law in the Milky Way. *The Astronomy and Astrophysics* 2019; 632 (A127): 1-13.

Barnabè M, Ciotti L, Fraternali F, and Sancisi R. Hydrostatic Models for the Rotation of Extra-planar Gas in Disk Galaxies. *The Astrophysics Journal* 2006; 446(1): 61-69.

Collins Joseph A, Benjamin, Robert A, Rand, and Richard J. Kinematics of Diffuse Ionized Gas Halos: A Ballistic Model of Halo Rotation. *The Astrophysical Journal* 2002; 578(1): 98-108.

Fraternali F, Oosterloo T, Sancisi R, and van Moorsel G. Gas accretion onto galaxies: models vs past and future observations. *The Astrophysical Journal* 2001: 562, L47.

Fraternali F, Binney JJ. Accretion of Gas on to Nearby Spiral Galaxies. *Monthly Notices of the Royal Astronomical Society* 2008; 386(2): 935–944.

Fraternali F, Marasco A, Marinacci F, Binney J. Ionized absorbers as evidence for supernova-driven cooling of the lower galactic corona. *The Astrophysical Journal Letters* 2013; 764(2): L21 1-5.

Fraternali F. Gas Accretion via Condensation and Fountains. Gas Accretion onto Galaxies. *In Astrophysics and Space Science Library* 2017; 430: 323-353.

Heald GH, Rand RJ, Benjamin RA, Bershady MA. Integral field unit observations of NGC 4202: kinematics of the diffuse ionized gas halo. *The Astrophysical Journal* 2007; 663(2): 933-947.

Houck JC, Bregman JN. Low-Temperature Galactic Fountains. *Astrophysical Jou*rnal 1990; 352(2): 506-521.

Kalberla PMW, McClure-Griffiths NM, Pisano DJ, Calabretta MR, Ford H, Alyson, Lockman, Felix J, Staveley-Smith L, Kerp J, Winkel B, Murphy T, Newton-McGee K. GASS: the Parkes Galactic all-sky survey II. Stray-radiation correction and second data release. *Astronomy and Astrophysic Journal* 2010; 521(A17): 1-13.

Kalberla PMW, Haud U. Highlight: Gass: The Parkes Galactic All-Sky Survey. III . *Astronomy and Astrophysics Journal* 2015: 578.

Kaufmann T, Mayer L, Wadsley J, Stadel J, and Moore B (2006) Cooling Flows within Galactic Haloes: the Kinematics and Properties of Infalling Multiphase Gas. *Monthly Notices of the Royal Astronomical Society* 370, 1612–1622.

Levine ES, Blitz L, Heiles C. The Warp and Spiral Arms of the Milky Way. *The astrophysics journal* 2006: 643.

McClure-Griffiths NM, Pisano DJ, Calabretta MR, Ford HA, Lockman FJ, Staveley-Smith L, Kalberla PMW, Bailin J, Dedes L, Janowiecki S, Gibson BK, Murpy T, Newton-McGee K. Gass: The Parkes Galactic All-Sky Survey. I. Survey Description, Goals, and Initial Data Release. *The Astrophysical Journal* 2009; 181(2): 398-412.

Olling R. The Highly Flattened Dark Halo of NGC 4244. *ASP Conference Series* 1996; 117: 82-89.

Oosterloo T, Fraternali F, Sancisi R. The Cold Gaseous Halo of NGC 891. The Astrophysical Journal 2007; 134(3): 1019-1036.

Rossa J, Dettmar RJ. An Hα survey aiming at the detection of extraplanar diffuse ionized gas in halos of edge-on spiral galaxies. *The Astronomy and Astrophysics* 2003; 406: 493 - 503.

Schaap WE, Sancisi R, Swaters RA. The vertical extent and kinematics of the HI in NGC 2403. *The Astronomy and Astrophysics Journal* 2000; 356: L49-L52.

Shapiro PR, Field GB. Consequences of a New Hot Component of the Interstellar Medium. *The Astrophysics Journal* 1976; 205: 762-765.

Veilleux S, Shopbell PL, Rupke DS, Bland-Hawthorn J, Cecil G. A search for very extended ionized gas in nearby starburst and active galaxies. *The Astronomical Journal* 2003; 126(5): 2185-2208.

Zschaechner LK, Rand R J, Heald GH, Gentile G, Kamphuis P. HALOGAS: HI observations and modeling of the nearby edge-on spiral galaxy NGC 4244. *The Astrophysics Journal* 2011: 740.

Zschaechner, Laura K, Rand Richard J. The HI Kinematics of NGC 4013: a Steep and Radially Shallowing Extra-planar Rotational Lag. *The Astrophysical Journal* 2015: 808(2).

Abdulrahman NA, Haddad NIA. Braggs, scherre, williamson–hall and ssp analyses to estimate the variation of crystallites sizes and lattice constants for zno nanoparticles synthesized at different temperatures. *NeuroQuantology* 2020; 18(1): 53-63.